High Q At Low And Medium Field

Gianluigi Ciovati

Thomas Jefferson National Accelerator Facility, Newport News, Virginia 23606
and Department of Physics, Old Dominion University, Norfolk, Virginia 23529

Abstract. The surface resistance of a bulk niobium superconducting rf cavity as function of the surface magnetic field is often characterized by three peculiar dependencies at low, medium and high field. Understanding the causes and the physics behind these anomalous behaviors is important to improve the performance of superconducting cavities used in particle accelerators. In this paper attention will be focused on low and medium field regions by presenting experimental results of several cavity test series and reviewing the models that try to explain these non-linearities of the surface resistance.

INTRODUCTION

The technology involved in the production of superconducting rf cavities made of bulk niobium has greatly evolved over the last ten years. In the last few years many single-cell and multi-cell cavities achieved peak surface magnetic fields close to the theoretical limit of niobium [1]. High-power testing of a superconducting cavity allows the exploration of non-linearities in the surface resistance R_s as a function of the peak surface magnetic field B_{peak} by measuring the quality factor Q_0 ($R_s=G/Q_0$, where G is the geometrical factor) as a function of B_{peak}. A typical plot of Q_0 vs. B_{peak} is characterized by an increase of the quality factor up to about 20 mT, followed by a slow decrease ("slope") of Q_0 up to about 90 mT when a strong degradation of Q_0 appears even in the absence of field emission ("Q-drop").

For accelerators operating in continuous wave (cw) mode, dynamic losses dominate the operating costs and to reduce them it is necessary to use cavities with a high quality factor at medium to high fields. Therefore, it is important to understand the physics behind the Q-variations with field to develop procedures that will minimize the rf losses at the operating accelerating gradient.

LOW FIELD Q-INCREASE

Experimental Results

The low field Q-increase is an increase (about 40%) of the quality factor Q_0 between 2 and 15-20 mT peak surface magnetic field. It has been observed in many tests in several laboratories but mainly on cavities with resonant frequency of the fundamental mode (TM_{010}) above 1 GHz. For cavities with frequency below 1 GHz, there exists few data at very low field and even in those cases the low field Q-increase was rarely found. Fig. 1 shows this effect measured on a TESLA[2] 9-cell cavity at DESY, a CEBAF Low Loss[3] single-cell measured at Jefferson Lab and a TESLA single-cell measured at Saclay.

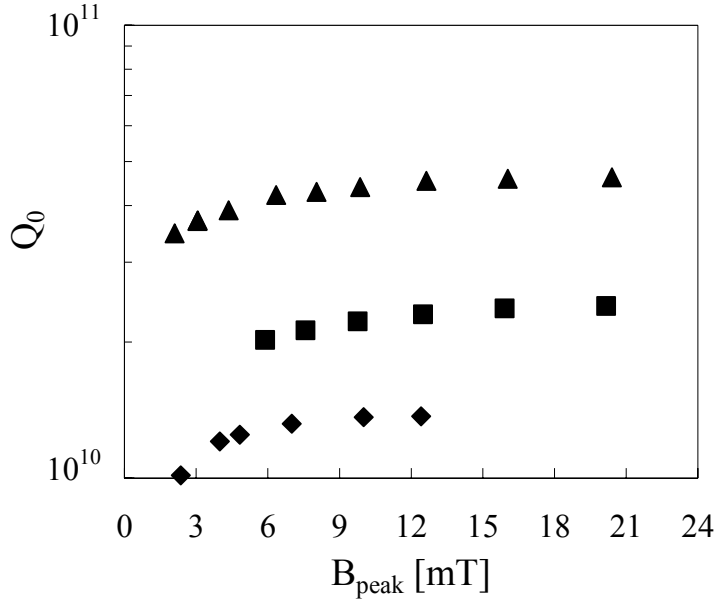

FIGURE 1. Low field Q-increase measured on a TESLA 1.3 GHz single-cell cavity at 1.7 K (triangles), a TESLA 1.3 GHz 9-cell cavity at 2 K (squares) and a CEBAF 1.48 GHz single-cell cavity at 2 K (diamonds).

It has been observed that the low-field Q-increase becomes more pronounced at lower temperatures: this effect, measured on a CEBAF Low Loss single-cell, is shown in Fig. 2. The error in Q_0 and B_{peak} is about 5%.

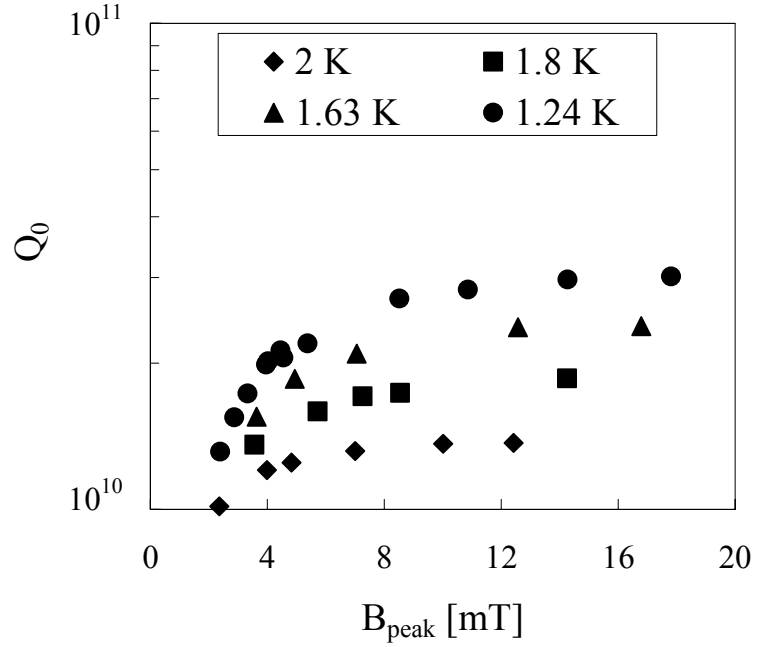

FIGURE 2. Low field Q-increase measured on a CEBAF Low Loss single-cell at different temperatures.

The B_{peak} at which the low field Q-increase saturates is also increasing at lower temperatures, as can be seen in Fig. 2. It is still possible to define a temperature independent residual resistance by subtracting the BCS surface resistance from the surface resistance at the saturation field at each temperature. The saturation peak magnetic field is inversely proportional to the temperature as shown in Fig. 3 along with the residual resistance.

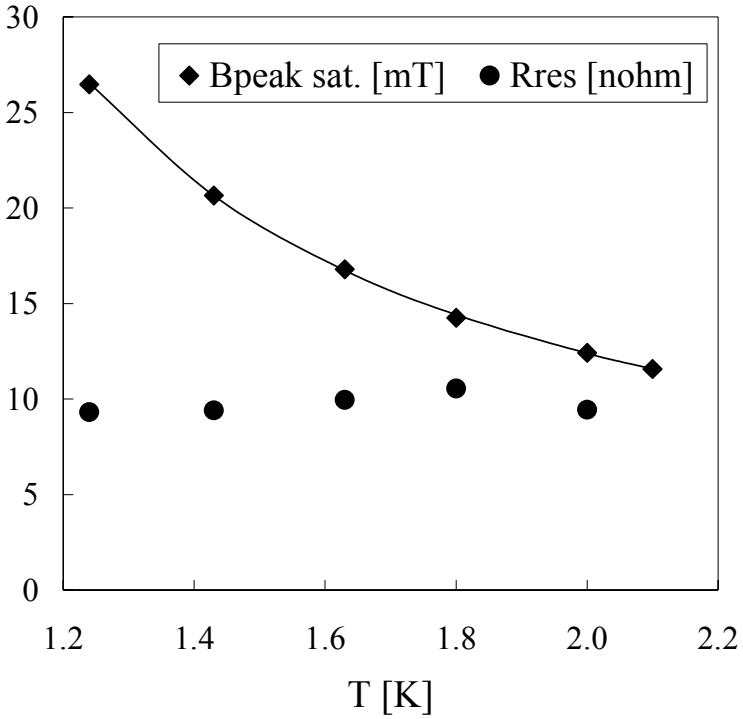

FIGURE 3. Peak magnetic field at which the low field *Q*-increase saturates (diamonds) and residual resistance (circles) as a function of temperature. The solid line corresponds to the fit $B_{peak}=1/(a+bT)$ with parameters *a* and *b* equal to -0.0325 1/mT and 0.0566 1/(mT K) respectively.

An additional result regarding the low field Q-increase is the fact that it is reduced by a high residual resistance. For example, this was observed on a CEBAF single-cell cavity where the residual resistance was increased by reducing the shielding of the Earth's magnetic field (Fig. 4).

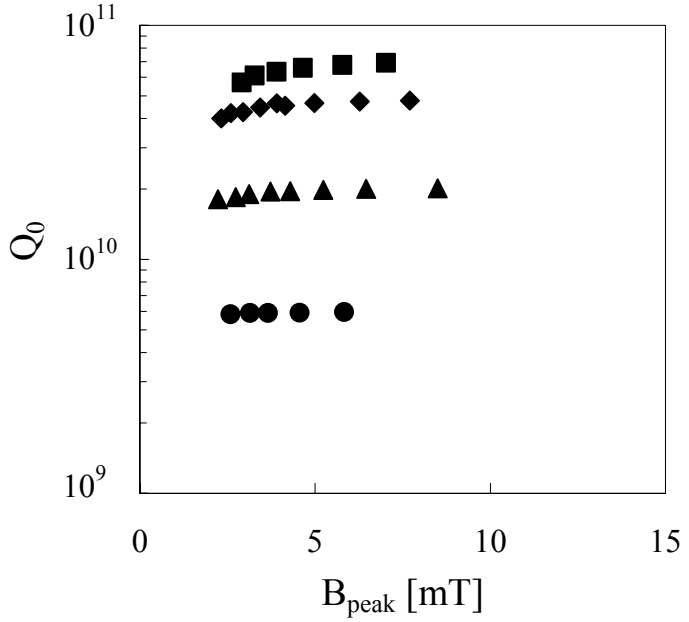

FIGURE 4. The low field *Q*-increase is reduced with increasing residual resistance: 4 nΩ (squares), 6 nΩ (diamonds), 13 nΩ (triangles) and 45 nΩ (circles).

A low temperature (100–150 °C) "in situ" bake enhances the low field *Q*-increase. Fig. 5 shows for example the low field Q-increase after the effect of baking a CEBAF single-cell cavity in UHV at 140 °C for 48 h.

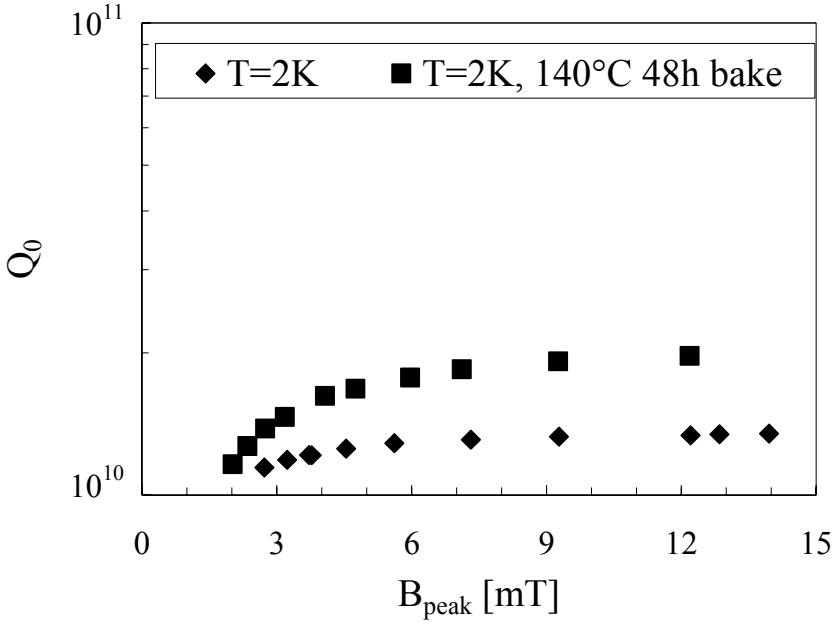

FIGURE 5. Low field *Q*-increase before (diamonds) and after (squares) baking a CEBAF single-cell cavity at 140 °C for 48 h.

Model Comparison

Halbritter's [4] model for this effect involves non-equilibrium superconductivity. In particular, at low temperature and low rf fields thermal equilibrium between quasiparticles and phonon bath is not achieved. To allow this phenomenon to take place two conditions are necessary: a mismatch between the quasiparticle absorption and relaxation rate and the presence of localized states inside the superconducting niobium energy gap.

At a temperature of 2 K, a resonant frequency of 1.5 GHz and rf magnetic field of 2 mT, quasiparticles absorb photons from the rf field at a rate $1/\tau_{ab} \approx 2$ GHz. Under the same conditions, the quasiparticles relaxation rate $1/\tau_r$, which is the sum of the quasiparticle-phonon scattering rate plus the recombination rate, is only about 0.03 GHz.

Surface analysis studies show that the niobium surface is covered by few monolayers of hydrocarbon and water followed by about 5 nm of niobium pentoxide Nb_2O_5. Underneath that, there are few monolayers of niobium suboxides NbO, NbO_2 as well as NbO_x (x<1) channels and clusters injected deeper into the niobium during the oxidation process [4]. These NbO_x clusters introduce localized states in the niobium energy gap, as shown in Fig. 6.

At low rf field, quasiparticles are confined in these localized states yielding an average gap Δ^* smaller than the energy gap of pure niobium. This results in a higher surface resistance. At higher rf field, quasiparticles are driven out of the localized states and occupy states above the niobium energy gap, causing a decrease of the surface resistance to the proper BCS value. Once quasiparticles have energies greater than the niobium gap they are in thermal equilibrium with the phonons because those can easily transfer their energy to the helium bath (at 2 K the phonon mean free path is greater than the cavity wall thickness).

Halbritter gives the following formula for the absorbed rf power per unit area *P*:

$$P = \frac{R_s}{2} H^2 = \int n_c \lambda I_r(\varepsilon) \mathrm{h}\omega \, d\varepsilon \tag{1}$$

where n_c is the density of states, λ is the rf penetration depth and I_r is the quasiparticle relaxation rate. Quasiparticles out of thermal equilibrium yield constant absorption, making the integral in (1) independent of the rf field amplitude. As a result the surface resistance is inversely proportional to the square of the rf field.

Fig. 7 shows the data of Fig. 1 fitted with the formula

$$R_s = \frac{a}{B_{peak}^2} + b \tag{2}$$

which shows very good agreement with the experimental data. The validity of this formula has been proved in many more experiments as reported in [5].

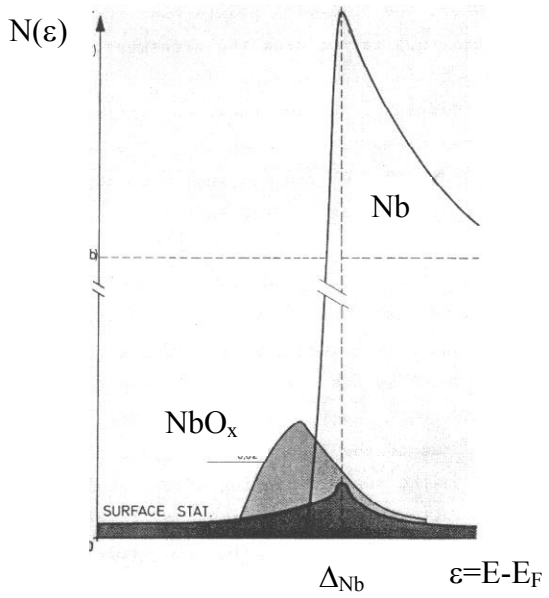

FIGURE 6. Density of states as a function of the energy of Nb (white area), NbO_x (grey area) and surface states (black area) from [5].

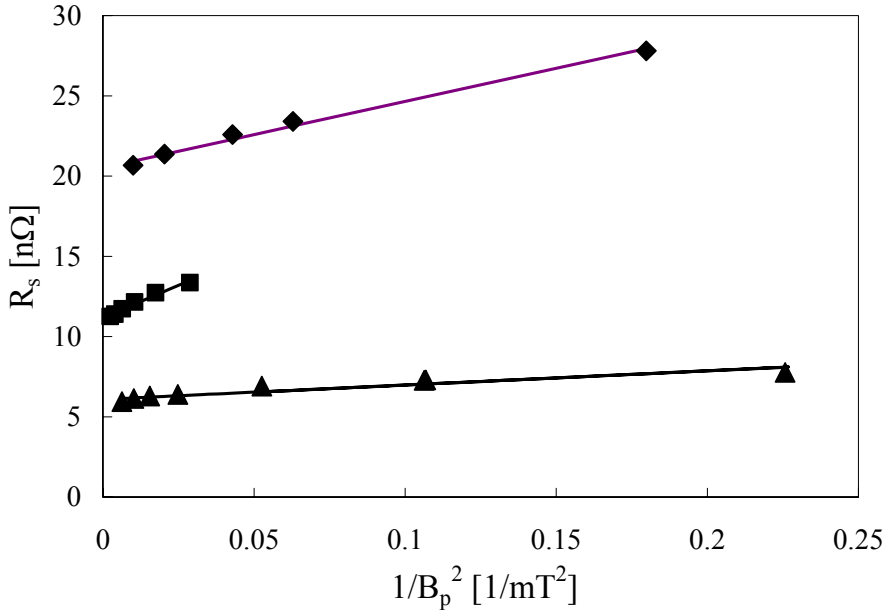

FIGURE 7. Surface resistance as function of $1/B^2_{peak}$ for the CEBAF Low Loss single-cell (diamonds), TESLA 9-cell (squares) and TESLA single-cell (triangles). The solid lines are the result of the fit with equation (2).

The values of the fit parameters *a* and *b* at different temperatures for the CEBAF Low Loss single-cell data of Fig. 2 are indicated in Table 1. There is no clear temperature dependence of *a*, while parameter *b* decreases at lower temperatures, reflecting the decrease of the BCS surface resistance.

TABLE 1. Fit parameters *a* and *b* of eq. (2) as function of temperature.

Temperature [K]	a [nΩ mT^2]	b [nΩ]
1.24	71.00	9.57
1.43	74.14	9.91
1.63	88.68	11.52
1.80	72.92	15.13
2.0	41.36	20.52
2.1	66.18	24.27

The model for the low field *Q*-increase can explain the temperature, baking and residual resistance dependences in the following way:

- the quasiparticle relaxation rate is proportional to $T^{3.5}$ so that at lower temperature there is a greater mismatch between absorption and relaxation rates, resulting in an enhancement of the low field *Q*-increase
- after low-temperature baking oxygen diffusion forms more niobium oxide clusters, increasing the density of localized states. This effect increases the term a/B^2_{peak} in (2)
- high residual resistance means a strong coupling between quasiparticles and phonons which prevents any mismatch and therefore reduces the low field *Q*-increase effect.

The model gives a fairly complete qualitative description of the experimental results but quantitative predictions are difficult, since it is strongly dependent on the surface morphology and the oxidation process.

MEDIUM FIELD Q-SLOPE

Beyond the field at which the low field *Q*-increase saturates, the cavity quality factor begins a gradual decrease. This continues up to a field where the degradation becomes stronger due to either field emission or *Q*-drop (typically 90 mT peak surface magnetic field). This region of gradual reduction is called "medium field *Q*-slope" and is a more or less pronounced common feature of all niobium superconducting cavities. Fig. 8 shows an example of this Q-slope on three different cavities: an SNS 6-cell β=0.61 805 MHz tested at 2.1 K, a TESLA 9-cell 1.3 GHz tested at 2 K and a CEBAF single-cell 1.48 GHz tested at 2 K.

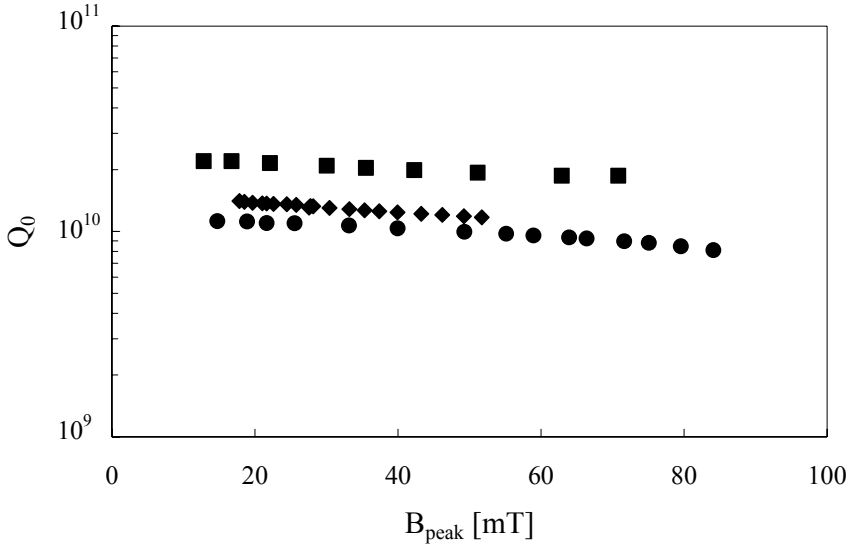

FIGURE 8. Medium field *Q*-slope for SNS 6-cell β=0.61 805 MHz at 2.1 K (diamonds), TESLA 9-cell 1.3 GHz at 2 K (squares) and CEBAF single-cell 1.48 GHz at 2 K (circles).

Experimental Results

The medium field *Q*-slope is temperature dependent: it increases significantly when the helium bath temperature is above the lambda point (T = 2.17 K), it has a minimum at about 2 K and it increases at lower temperatures [6, 7]. This dependence is shown in Fig. 9.

Low-temperature baking also seems to affect the medium field *Q*-slope and, in particular, seems to depend on the baking conditions: at Jefferson Lab and DESY, baking is done by flowing hot nitrogen and air on the outer surface of the cavity while at Saclay hot helium gas is used. The medium field *Q*-slope degradation after baking is less pronounced in cavities measured at Saclay [8]. Fig. 10 shows an example of this effect measured on a CEBAF single-cell cavity at 2 K [5].

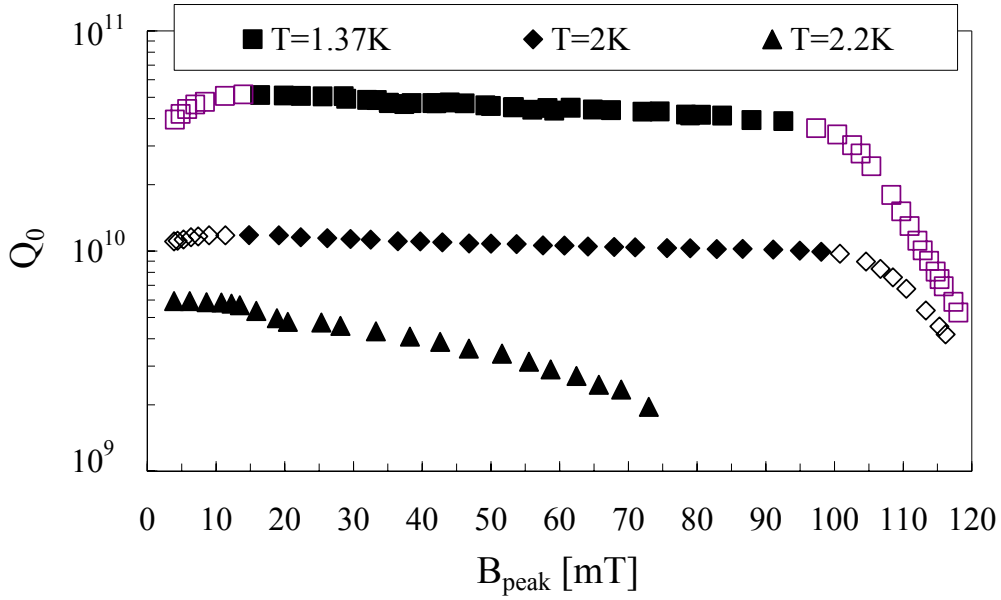

FIGURE 9. Temperature dependence of the medium field Q-slope (solid symbols) measured on a CEBAF single-cell cavity.

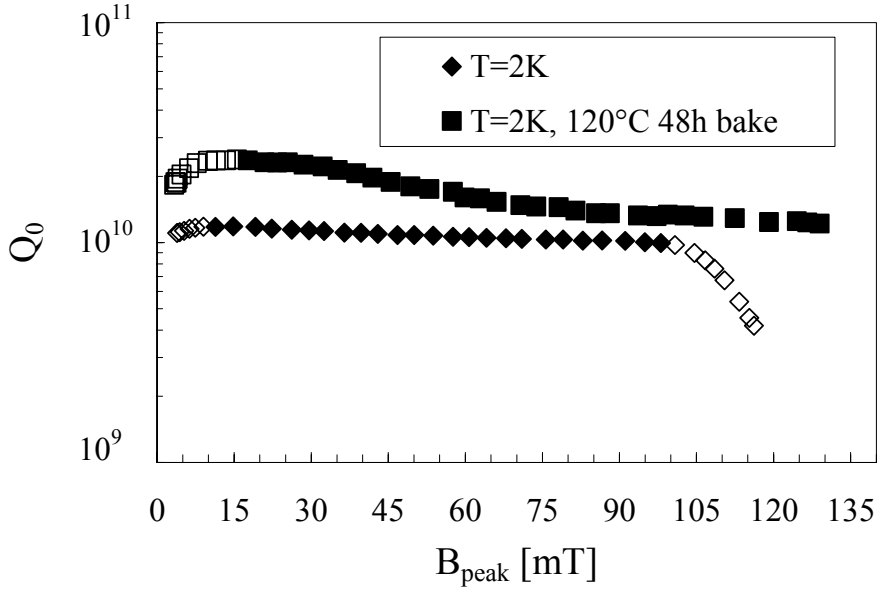

FIGURE 10. Medium field Q-slope (solid symbols) measured before and after baking on a CEBAF single-cell cavity.

Another treatment that influences the medium field *Q*-slope is post-purification of the cavity obtained by heating the cavity in a vacuum furnace at about 1200–1400 °C in the presence of titanium as a solid state getter. In many cases the *Q*-slope is reduced after such treatment [9].

Models Comparison

A model of the medium field *Q*-slope by Halbritter [10] involves heating of the rf surface to a temperature above the helium bath temperature due to the niobium-helium thermal resistance. The surface resistance is expressed as a Taylor series with even exponents of the peak surface magnetic field:

$$R_s\left(T, B_{peak}\right) = R_{s0}\left[1+\gamma\left(T\right)\left(\frac{B_{peak}}{B_c}\right)^2 + O\left(B_{peak}^4\right)\right] \tag{3}$$

where R_{s0} is the surface resistance at about 15 mT, B_c = 200 mT is the niobium critical field and T is the He bath temperature. The medium field *Q*-slope is represented by the variable $\gamma(T)$. γ = 1 implies a 25% increase in surface resistance between 15 and 100 mT peak surface magnetic field. From Ginzburg-Landau theory, the value of gamma should be lower than 0.2 but it is enhanced by the niobium thermal resistance. Halbritter gives the following approximated formula for $\gamma(T)$:

$$\gamma\left(T\right) \approx R_{BCS}\left(T\right)\frac{B_c^2\Delta}{2kT^2}\left(\frac{d}{\kappa}+R_K\right) \tag{4}$$

where κ and R_K are the niobium thermal conductivity and Kapitza resistance respectively, d is the wall thickness.

Another possible cause for the medium field *Q*-slope is the presence of oxide channels, especially along grain boundaries, creating weak links in the rf penetration field region. The critical field of Nb-NbO_x-Nb weak links is about 15 mT which is comparable to the peak surface field where the *Q*-slope starts. Above this field Josephson fluxons start to penetrate and generate nucleation and pinning (hysteresis) losses.

According to Halbritter [11] these hysteresis losses are expressed by a linear relationship between surface resistance and rf field $R_s \propto \omega B_{rf}$. Data have been analyzed using the following simple equation:

$$R_s = a + bB_{peak} \tag{5}$$

where the parameter b represent the medium field *Q*-slope.

Cavity Production Results

In this section the values of the medium field *Q*-slope for three cavity production series will be compared with the predictions of equations (3) and (5). Over the last two years, Jefferson Lab has been involved with the production and testing of about 80 6-cell 805 MHz cavities of two different β values (β=2L/λ where L is the cell length and λ is the wavelength of the fundamental mode) for the SNS proton linac [12]. In addition, three cryomodules, two for the CEBAF upgrade (SL21 and NL11) and one for the FEL upgrade (FEL3), each made of eight 7-cell 1.5 GHz cavities have been built [13]. DESY has been working on the production of 9-cell 1.3 GHz cavities for TTF [14] and their most recent data will be presented.

Fig. 11 shows the values of γ and b for the SNS β=0.61 cavity production. The average values are γ = 3.4 ± 1.2 and b = 0.087 ± 0.031 nΩ/mT. After cavity MB26, a new preparation procedure was adopted consisting of more buffered chemical polishing (200 μm instead of 50 μm material removal) after hydrogen degassing in a vacuum furnace at 600 °C for 10 h, longer water rinsing after chemical treatment and longer high-pressure water rinsing (2x4 h instead of 2x1 h). This had no significant effect on the medium field Q-slope while it helped in reducing the residual resistance from an average of 9.3 ± 3.5 nΩ to 4.8 ± 1.1 nΩ and increasing the field emission onset by about 6 MV/m peak surface electric field.

Fig. 12 shows the values of γ and b for the β=0.81 cavities tested to date. The average values are γ = 4.86 ± 2.53 and b = 0.114 ± 0.076 nΩ/mT. The average residual resistance is 7.8 ± 2.7 nΩ. It is interesting to note the larger value of γ for HB32 and HB38 which were baked at 120 °C for 48 h.

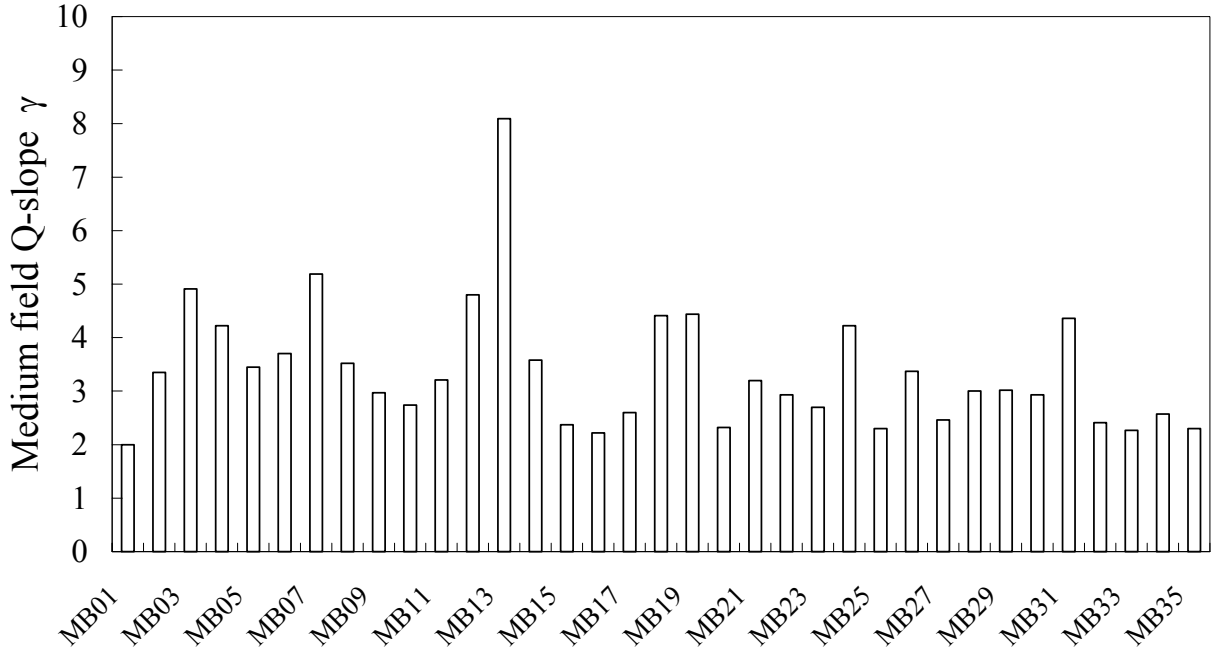

FIGURE 11. Medium field Q-slope γ for the 35 SNS β=0.61 cavities tested at 2.1 K.

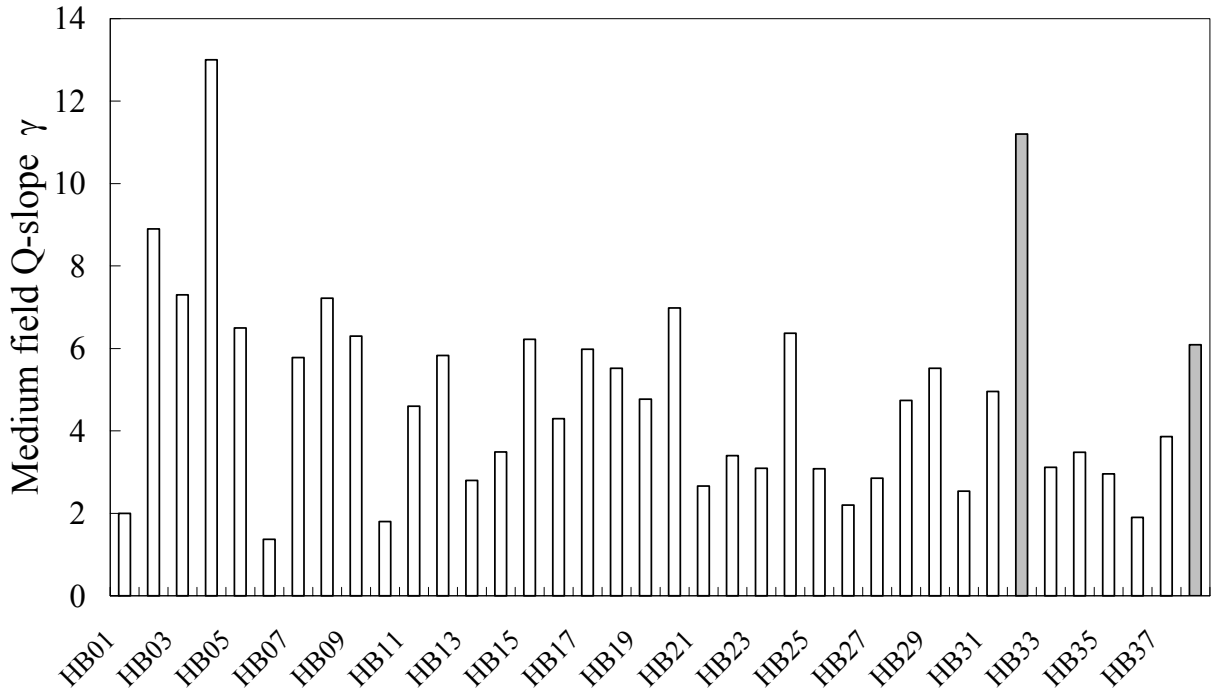

FIGURE 12. Medium field Q-slope γ for 38 SNS β=0.81 cavities tested at 2.1 K. The grey bars refer to cavities which were baked "in situ" at 120 °C for 48 h.

Fig. 13 shows the medium field Q-slope γ for the CEBAF cavities: the ones installed in the SL21 cryomodule were characterized by strong contamination and early field emission onset but the performances kept improving over time reaching very low values of γ for the NL11 (named also "Renascence") production. For the latter, the improved procedures from the SNS cavity production were adopted. Again, for cavities LL02 and LL04 the slope

increased by about a factor of three after "in situ" baking at 120 °C for 48 h. The average values of γ and b are indicated in Table 2 along with the average values for the other cavity production runs discussed in this article. The average value of residual resistance is 6.8 ± 4.6 nΩ.

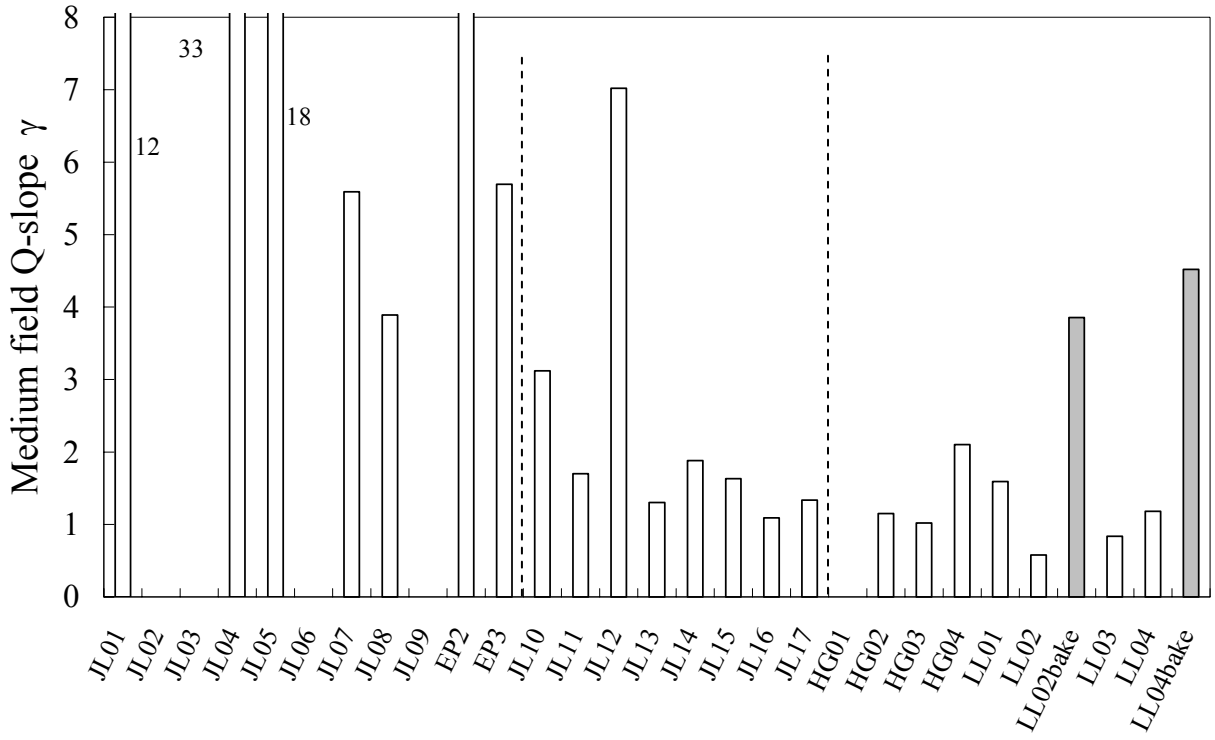

FIGURE 13. Medium field Q-slope γ for CEBAF cavities. The dashed line separates the cavities produced for cryomodules SL21, FEL3 and NL11. The cavities for NL11 were tested at 2.07 K while the rest were tested at 2 K. The grey bars refer to cavities that were baked at 120 °C for 48 h.

Fig. 14 shows the medium field Q-slope γ for TESLA cavities [15] measured at 2 K. There is no significant difference between cavities that had only the hydrogen degassing at 800 °C for 2 h and the ones that were post-purified at 1350 °C for 3 h with Ti. In both cases, however, the medium field Q-slope increased after baking at 120 °C for 48 h except for cavity AC80.

The average value of the medium field Q-slope is: $\gamma = 1.73 \pm 1.67$ and $b = 0.090 \pm 0.176$ nΩ/mT.

TABLE 2. Average medium field Q-slope γ and b and fit correlation factors r^2 for different cavity productions.

Cavity Type	γ	r^2	b [nΩ/mT]	r^2
SNS β=0.61	3.38 ± 1.20	0.926	0.087 ± 0.310	0.907
SNS β=0.81	4.86 ± 2.53	0.865	0.114 ± 0.076	0.848
CEBAF/SL21	12.3 ± 10.2	0.917	0.360 ± 0.295	0.898
CEBAF/FEL3	2.38 ± 1.97	0.893	0.092 ± 0.079	0.849
CEBAF/NL11	1.91 ± 1.04	0.901	0.068 ± 0.045	0.930
TESLA	1.73 ± 1.67	0.964	0.090 ± 0.176	0.966

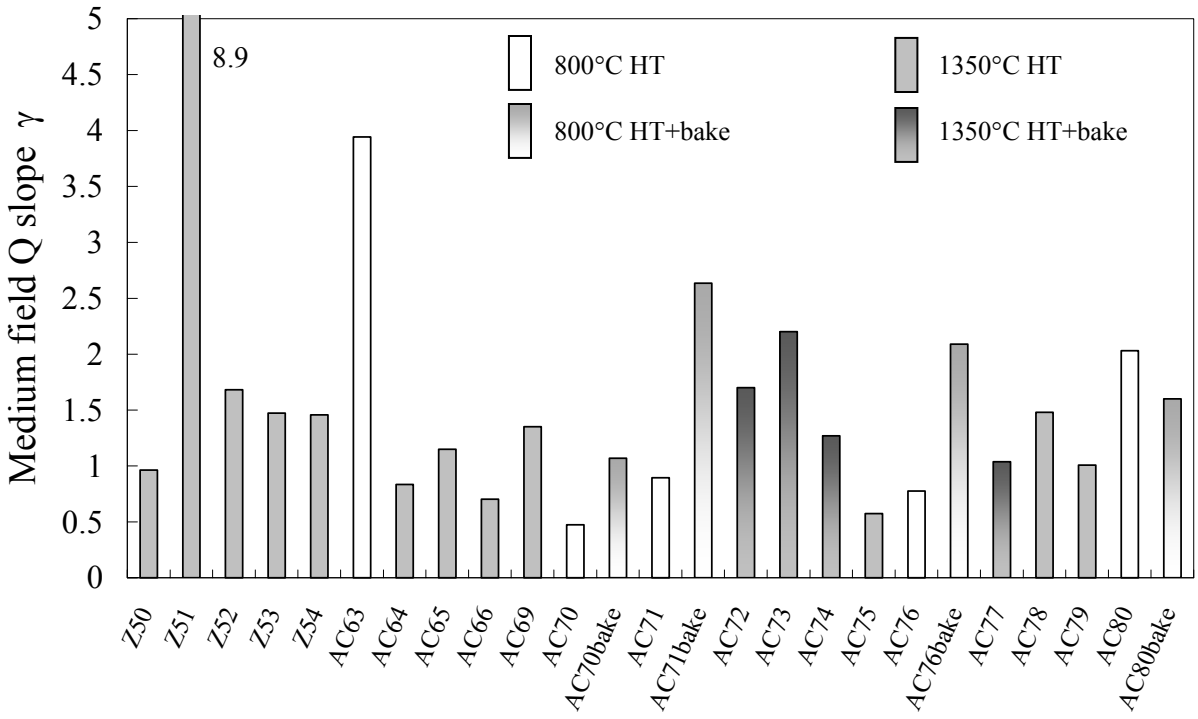

FIGURE 14. Medium field Q-slope γ for TESLA cavities tested at 2 K.

It appears from the data analysis of the medium field Q-slope that for strong slopes (γ values greater than about 2) the quadratic dependence of equation (3) gives the best fit, suggesting heating as the main cause for the slope. For low values of slope and after baking, the linear dependence (5) becomes a good data fit and, in particular, after baking is consistently better than the quadratic fit. This might suggest that when the heating is low, hysteresis losses become measurable and dominate the slope due to an increased number of weak-links after baking. This effect is shown (Fig. 15) by plotting in the surface resistance as function of the peak surface magnetic field before and after baking for the data shown in Fig. 10.

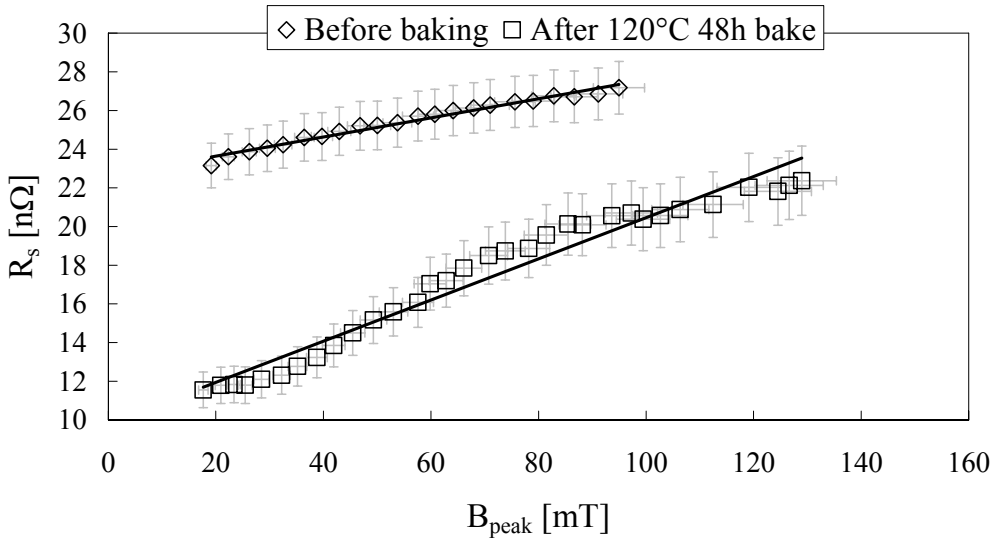

FIGURE 15. Surface resistance as function of the peak surface magnetic field for the data of Fig. 10. Solid lines represent fits with linear equation (5), showing the slope increase after baking.

Medium Field Q-slope Analysis

The experimental data suggest that the main contribution to the medium field *Q*-slope comes from heating of the rf surface due to the poor niobium-helium thermal interface. This is supported by the fact that the slope is temperature dependent, being high above 2.17 K when niobium is cooled by He I, and below 2 K when the Kapitza resistance dominates. Furthermore, cavities built with thicker niobium show stronger slope than thinner ones (SNS cavities are 3.8 mm thick while CEBAF and TESLA cavities are 2.5-2.8 mm thick) and cavities with higher thermal conductivity generally show a reduced slope. On the other hand, thermal models predict significant smaller slopes than experimentally measured [16, 17] and low-frequency quarter-wave and half-wave resonators show less marked temperature dependence of the medium field *Q*-slope [18].

The importance of the Kapitza resistance on the *Q*-slope at 2 K is not clear: the stronger slope for cavities baked with hot nitrogen/air than for cavities baked with hot helium could be related to a higher Kapitza resistance, although there are no direct measurements after baking; but cavities whose outer surface was chemically etched (TESLA) show comparable *Q*-slope to cavities that did not receive such treatment (CEBAF). Measurements of Kapitza resistance [19] show lower values for chemically etched surfaces.

Another possible source of additional heating of the rf surface could be contamination of the inner surface from particulate or chemical residues as was probably the case for CEBAF/SL21 cavities. On the other hand the cavity production data shows that there is no correlation between *Q*-slope and residual resistance.

Finally, the experimental data seems to sustain the hypothesis of hysteresis losses due to oxides weak-links which grow after low-temperature baking.

CONCLUSIONS

Understanding non-linear behavior of the *Q*-value as a function of rf field level is very important to reduce the cryogenic losses of high-gradient superconducting cavities operating in cw mode.

Measurements of low field *Q*-increase are well described by a model involving quasiparticle-phonon non-equilibrium enforced by localized states within the niobium energy gap. Low-temperature baking seems to be effective in enhancing this effect.

There exist no models that can quantitatively account for the value of the medium field *Q*-slope. Experimental data indicate that material properties influencing the niobium-helium thermal interface such as thermal conductivity, wall thickness, and Kapitza resistance play an important role. Surface contamination and hysteresis losses appear also to be possible causes. A general remark is that the results obtained from cavity productions show large scatter in *Q*-slope data and this is an additional indication that the sources of the slope and the parameters that influence it are not yet clear and under control. To maintain the improvement of the quality factor by low-temperature baking at high gradient it is important to develop a baking procedure that will minimize its impact on the medium field *Q*-slope. From the theoretical point of view, recent studies [20] show that there might be an intrinsic dependence of the BCS surface resistance on the rf field, which could account for part of the *Q*-slope.

ACKNOWLEDGMENTS

I would like to acknowledge J. Halbritter and P. Kneisel for many useful discussions and suggestions. This work was supported by the U.S. DOE contract No. DE-AC05-84ER40150.

REFERENCES

1. Lilje L., *Proceedings of the 2004 European Particle Accelerator Conference*, Lucerne, Switzerland, 2004, to be published.
2. Brinkmann R. et al., *TESLA – Technical Design Report,* DESY, Amburg, Germany, 2001.
3. Kneisel P. et al., *Proceedings of the 2004 Linear Accelerator Conference,* Lubeck, Germany, 2004, to be published.
4. Halbritter J., *Proceedings of the 10th Workshop on RF Superconductivity,* Tsukuba, Japan, 2001, pp. 292-301.
5. Halbritter J., *Proceedings of the 1th Workshop on RF Superconductivity,* Karlsruhe, Germany, 1980, pp. 190-214.
6. Ciovati G., *J. of Appl. Phys.*, **96** No. 3, 1591-1600 (2001).
7. Kneisel P., *Proceedings of the 8th Workshop on RF Superconductivity*, Abano Terme, Italy, 1997, p. 463.

8. Visentin B., *Proceedings of the 11th Workshop on RF Superconductivity*, Travemuende, Germany, 2003, to be published.
9. Safa H., *Proceedings of the 10th Workshop on RF Superconductivity,* Tsukuba, Japan, 2001, pp. 279-286.
10. Halbritter, J., *Proceedings of the 38th Eloisitron Workshop*, Erice, Italy, 1999, p. 59.
11. Halbritter J., *J. Supercond.* **8**, 691-703 (1995).
12. www.sns.gov
13. Valente A.-M., *Proceedings of the 2004 European Particle Accelerator Conference*, Lucerne, Switzerland, 2004, to be published.
14. Moeller W.-D. *Proceedings of the 10th Workshop on RF Superconductivity,* Tsukuba, Japan, 2001, pp. 212-215.
15. http://tesla.desy.de/~oracle/ttf_gui_home.htm
16. Reschke D., *Proceedings of the 8th Workshop on RF Superconductivity*, Abano Terme, Italy, 1997, pp. 385-394.
17. Saito K., *Proceedings of the 11th Workshop on RF Superconductivity*, Travemuende, Germany, 2003, to be published.
18. Kelly M., these proceedings.
19. Boucheffa A., Francois M. X., *Proceedings of the 7th Workshop on RF Superconductivity*, Gif sur Yvette, France, 1995, pp. 659-663.
20. Gurevich A., these proceedings.